Available online at www.sciencedirect.com

SCIENCE DIRECT®

Journal of Computational and Applied Mathematics 196 (2006) 132–149

JOURNAL OF COMPUTATIONAL AND APPLIED MATHEMATICS

www.elsevier.com/locate/cam

Application of space–time CE/SE method to shallow water magnetohydrodynamic equations

Shamsul Qamar*, Gerald Warnecke

Institute for Analysis and Numerics, Otto-von-Guericke University PSF 4120, D-39106 Magdeburg, Germany

Received 30 January 2005; received in revised form 29 July 2005

Abstract

In this article we apply a space–time conservation element and solution element (CE/SE) method for the approximate solution of shallow water magnetohydrodynamic (SMHD) equations in one and two space dimensions. These equations model the dynamics of nearly incompressible conducting fluids for which the evolution is nearly two-dimensional with magnetic equilibrium in the third direction. In this article we are using a variant of the CE/SE method developed by Zhang et al. [A space–time conservation element and solution element method for solving the two-dimensional unsteady Euler equations using quadrilateral and hexahedral meshes, J. Comput. Phys. 175 (2002) 168–199]. This method uses structured and unstructured quadrilateral and hexahedral meshes in two and three space dimensions, respectively. In this method, a single conservation element at each grid point is employed for solving conservation laws no matter in one, two, and three space dimensions. The present scheme use the conservation element to calculate flow variables only, while the gradients of flow variables are calculated by central differencing reconstruction procedure. We give both one- and two-dimensional test computations. A qualitative comparison reveals an excellent agreement with previous published results of wave propagation method and evolution Galerkin schemes. The one- and two-dimensional computations reported in this paper demonstrate the remarkable versatility of the present CE/SE scheme.

MSC: 76W05; 35L65; 65M06; 35L45; 35L67

Keywords: Shallow water magnetohydrodynamic equations; CE/SE method; Conservation laws; Hyperbolic systems; Discontinuous solutions

1. Introduction

Shallow-water problems occur in a wide variety, such as atmospheric flows, tides, storm surges, river and coastal flows, lake flows, tsunamis. They describe flows of fluids with free surface under the influence of gravity, where the vertical dimension is much smaller than any typical horizontal scale. Numerical simulation is an effective tool to solve them and a great variety of numerical methods are available in the literature, see for example [10,14] and references therein.

Shallow water magnetohydrodynamic (SMHD) equations were recently proposed in [8] as a model for phenomena in solar tachocline [13]. The tachocline is a thin layer in the solar interior, making the transition between the convection

* Corresponding author. Tel.: +49 3916712877; fax: +49 3916718073.
E-mail addresses: Shamsul.Qamar@Mathematik.Uni-Magdeburg.DE (S. Qamar), Gerald.Warnecke@Mathematik.Uni-Magdeburg.DE (G. Warnecke).

0377-0427/$ - see front matter © 2005 Elsevier B.V. All rights reserved.
doi:10.1016/j.cam.2005.08.014

zone, which rotates in a differential way, and the uniformly rotating radiative interior, see [13]. The SMHD system is a magnetohydrodynamic (MHD) analog to the classical shallow water equations. These equations are the approximation of the ideal MHD equations in the situation of a free-surface, shallow, and electrically conducting fluid that has constant density and is in magnetohydrostatic balance in the vertical direction. Gilman [8] gives a brief phenomenological derivation of the SMHD equations, and sketches some of their properties. De Sterck [7] has derived the basic properties of SMHD equations as a nonlinear system of hyperbolic conservation laws. Furthermore, Rossmanith [12] in his PhD thesis has also derived the SMHD with further details. Because of the constant density assumption, all sound waves are filtered out of the SMHD equations and the resulting SMHD system is different from the full ideal MHD equations with eigen structure which is less complicated. In contrast to full MHD system, the SMHD system is a convex and strictly hyperbolic system. Moreover, in the case of the two-dimensional MHD system, nonuniqness of the solution, the so-called compound wave, has been observed. However like MHD systems, the SMHD system also require a special treatment of divergence-free constraint. It is instructive to consider the SMHD system as an important first step in solving ideal MHD system. Presently the use of the SMHD in various applications is being explored. Gilman [8] anticipates that the SMHD equations may play a role for tachocline-type astrophysical problems that is similar to the role played by the shallow water equations for describing the Earth's atmosphere and oceans. The SMHD equations may also be applicable to problems involving the free surface flow, Toro [14], of conducting fluids in laboratory and industrial environments.

In this article we implement the space–time conservation element solution element (CE/SE) method to solve the SMHD equations. The CE/SE method, originally proposed by Chang [2,5,16,6], is new numerical frame for conservation laws. This method is not an incremental improvement of a previously existing CFD method, and it differs substantially from other well-established methods. The CE/SE method has many nontraditional features, including a unified treatment of space and time, the introduction of conservation element (CE) and solution element (SE), and a novel shock capturing strategy without using Riemann solvers. To date numerous highly accurate solutions have been obtained by using CE/SE method, see [5,16,6,17–20] and references therein.

The CE/SE method is a family of schemes, i.e., the a scheme, the $a-\varepsilon$ scheme, and the $a-\alpha$ scheme. The a scheme determines the space–time geometry of the numerical mesh employed. The $a-\varepsilon$ and the $a-\alpha$ schemes are extensions of a scheme for nonlinear equations and for shock capturing. In the CE/SE method, the space–time domain of interest is first divided into many conservative elements (CEs). These conservation elements are nonoverlapping space–time domains such that the computational domain is the union of these subdomains. The flux conservation can be enforced over each of these subdomains and can also be applied to their union. In each SE, flow variables are assumed continuous. A first-order Taylor series is then used in [2] to discretize the flow variables. Thus the scheme is second-order accurate. Across the boundaries of neighboring SEs, flow discontinuities are allowed. Flow variables are calculated through a local space–time flux balance, which is enforced by integrating over the surfaces of CE. Unlike SEs, various CEs could be imposed for local and global space–time flux balance. In the nondissipative a scheme, the number of the CEs employed marches the number of unknowns designated by the scheme. In addition to flow variables, the spatial gradients of flow variables are also treated as unknowns. As a result, two CE are used to solve a one-dimensional conservation equation, because the variable w and its spatial derivative w_x are unknowns. Similarly three CEs are used for two-dimensional equations, because w w_x and w_y are the unknowns, and four CEs are for three-dimensional conservation equation. As shown in [5], triangles and tetrahedrons are the basic mesh stencils to construct the necessary CEs for two- and three-dimensional equations. Unlike the modern upwind scheme, flow variable distribution inside SE is not calculated through a reconstruction procedure using its neighboring values at the same time level. Instead they are calculated as a part of local space–time flux conservation.

In this paper we consider the variant CE/SE method proposed in [17]. The present method uses only one CE at each grid point in one, two and three space dimensions. In contrast to the original a-scheme, the CE in the present method is used only to calculate the flow variables, while the spatial gradients of the flow variables are calculated by a central differencing method. This method is similar to $a-\varepsilon$ schemes for $\varepsilon = 1/2$, see [5]. Furthermore, only one CE per mesh point is also used in the recently developed Courant number insensitive schemes, see [3,4]. For the two-dimensional case the present method allows the use of quadrilaterals and/or polygons in either structured and unstructured meshes. The one-dimensional case of the present scheme is a special case of the Chang's original scheme [2]. Like other upwind and central schemes, the present scheme is not divergence-free. Therefore we need to impose the divergence-free condition by using the projection method, see [1,15,12]. We will explain this method in the coming section. The reader will see in Section 4 that the discrete divergence of the magnetic field for all problems presented here are quite small and hence

does not considerably effect the numerical results. However, there may exist some physical problems in connection to the present model where one must use the divergence cleaning procedure.

The paper is organized as follows. In Section 2, we present the SMHD equations in two space dimensions. In Section 3, we recall the derivation of the current CE/SE method on a two-dimensional regular rectangular grid. Section 4 includes five numerical test problems demonstrating the usefulness of the CE/SE method for the SMHD equations. In Section 5, we give conclusions and remarks.

2. The SMHD equations

The SMHD equations were proposed in [8]. Afterwards, Sterck [7] and Rossmanith [12], among others, worked on these equations. The SMHD equations can be derived from the ideal MHD equations. This system model the dynamics of a free surface fluid that has homogeneous density and is in magnetohydrostatic balance in the vertical direction. A detailed derivation is given in [12]. This gives a system of $m = 5$ equations in two space dimensions, which is given by

$$\partial_t \mathbf{w} + \partial_x f(\mathbf{w}) + \partial_y g(\mathbf{w}) = c(\mathbf{w}), \tag{2.1}$$

where

$$\mathbf{w} = \begin{pmatrix} h \\ hu_1 \\ hu_2 \\ hB_1 \\ hB_2 \end{pmatrix}, \quad f(\mathbf{w}) = \begin{pmatrix} hu_1 \\ hu_1^2 - hB_1^2 + \frac{1}{2}gh^2 \\ hu_1u_2 - hB_1B_2 \\ 0 \\ hu_1B_2 - hu_2B_1 \end{pmatrix}, \tag{2.2}$$

$$g(\mathbf{w}) = \begin{pmatrix} hu_2 \\ hu_1u_2 - hB_1B_2 \\ hu_2^2 - hB_2^2 + \frac{1}{2}gh^2 \\ hu_2B_1 - hu_1B_2 \\ 0 \end{pmatrix}, \quad c(\mathbf{w}) = \begin{pmatrix} 0 \\ -gh\partial_x b \\ -gh\partial_y b \\ 0 \\ 0 \end{pmatrix}, \tag{2.3}$$

together with the intrinsic constraint

$$\nabla \cdot (h\mathbf{B}) = 0. \tag{2.4}$$

Here $g > 0$ is the gravitational constant, and $b = b(\mathbf{x})$ describes the bottom topography. In the current paper, we restrict ourselves to the case of a flat bottom, i.e. $b = \text{const.}$ so that the system is homogeneous. We deal with the numerical approximation of the time-dependent system (2.1) and derive the numerical approximation of the divergence constraint (2.4). We found that this numerical scheme is not inherently divergence-free hence we need some divergence cleaning procedure. For that purpose we use the projection method, see [1,12,15]. This is conceptually the easiest and probably widely used method. The idea is to predict the value of the magnetic field through some cell-centered finite volume method and then correct this value by projecting it to its divergence-free subspace. A single step of our method gives

$$[h^n, (hu_1)^n, (hu_2)^n, \mathfrak{B}_1^n, \mathfrak{B}_2^n] \longrightarrow [h^{n+1}, (hu_1)^{n+1}, (hu_2)^{n+1}, \mathfrak{B}_1^*, \mathfrak{B}_2^*], \tag{2.5}$$

where $\mathfrak{B} = (\mathfrak{B}_1, \mathfrak{B}_2)^{\mathrm{T}} = (hB_1, hB_2)^{\mathrm{T}}$. Strictly speaking this is the depth-averaged magnetic field multiplied by the depth of the fluid. We can decompose the predicted magnetic field in the following way:

$$\mathfrak{B}^* = \nabla \times \mathbb{A} + \nabla\phi, \tag{2.6}$$

where $\mathbb{A}$ is magnetic potential. Taking the divergence of both sides yields

$$\nabla^2\phi = \nabla \cdot \mathfrak{B}^*. \tag{2.7}$$

If this Poisson equation for the potential is solved, then the divergence-free magnetic field at time $t = t_{n+1}$ is given by

$$\mathfrak{B}^{n+1} = \mathfrak{B}^* - \nabla\phi. \tag{2.8}$$

The standard approach is to approximate $\nabla\phi$ and $\nabla^2\phi$ by the following finite difference operators in order to make $\nabla\phi$ a cell centered quantity:

$$[\nabla\phi]_{ij} \approx \left(\frac{\phi_{i+1,j}-\phi_{i-1,j}}{2\Delta x}, \frac{\phi_{i,j+1}-\phi_{i,j-1}}{2\Delta y}\right), \tag{2.9}$$

$$[\nabla^2\phi]_{ij} \approx \frac{\phi_{i+2,j}-2\phi_{i,j}+\phi_{i-2,j}}{4\Delta x^2} + \frac{\phi_{i,j+2}-2\phi_{i,j}+\phi_{i,j-2}}{4\Delta y^2}. \tag{2.10}$$

This approach guarantees that the following discrete divergence is identically zero:

$$[\nabla\cdot\mathfrak{B}]_{ij} \approx \left(\frac{[\mathfrak{B}_1]_{i+1,j}-[\mathfrak{B}_1]_{i-1,j}}{2\Delta x} + \frac{[\mathfrak{B}_2]_{i,j+1}-[\mathfrak{B}_2]_{i,j-1}}{2\Delta y}\right). \tag{2.11}$$

3. Derivation of (CE/SE) method

Here we give a brief overview of [17] which follow the concepts in [2,6]. Here we will derive the two-dimensional CE/SE method for a regular rectangular grid. For more detailed derivation on generalized grid we refer the reader to [17]. Let $x_1 = x$, $x_2 = y$, and $x_3 = t$ be the coordinates of a three-dimensional Euclidean space E_3. Now Eq. (2.1) is equivalent to the integral equation

$$\oint_{S(V)} \mathbf{h}_m \cdot \mathrm{d}\mathbf{S} = 0, \quad m = 1, 2, 3, 4, 5, \tag{3.1}$$

where m indicates the number of equations and $S(V)$ is the boundary of an arbitrary space–time region V in E_3, and the space–time current vector $\mathbf{h}_m = (f_m, g_m, w_m)$. Eq. (3.1) is enforced over a space–time region, called CE, in which the discontinuities of the flow variables are allowed. The actual numerical integration is carried out in discrete sense by using SEs in which the flow variables are assumed smooth and can be approximated by a specific function.

3.1. The space–time geometry of the CE and SE

To proceed, we first divide the entire computational domain into nonoverlapping uniform convex quadrilateral cells, see Fig. 1. The centroid of each cell is denoted by a circle symbol, which is also the grid point in the modified CE/SE

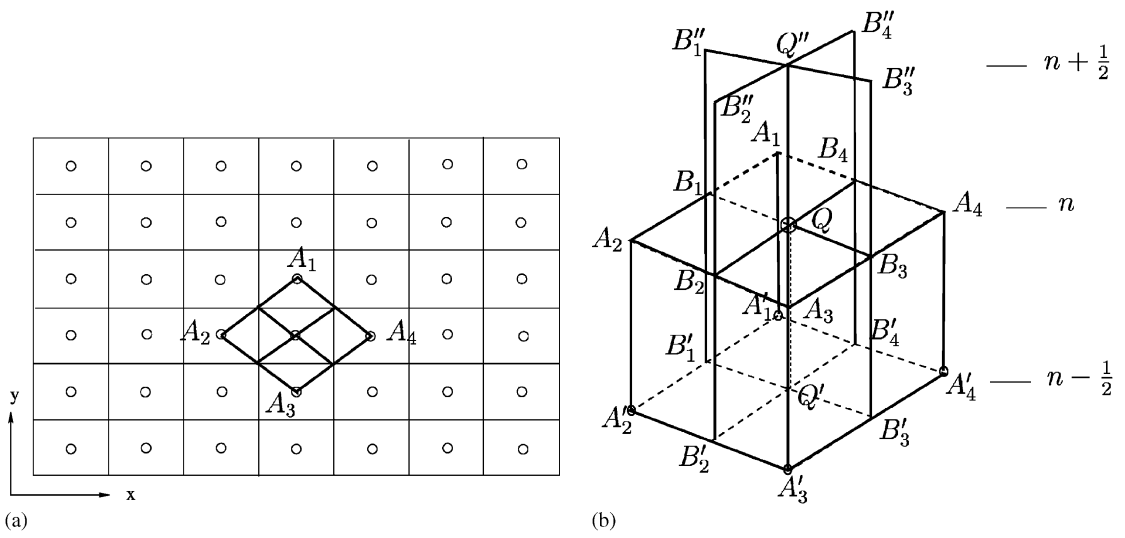

Fig. 1. Space–time geometry of the modified CE/SE method: (a) representative grid points in an x–y plane, (b) the definitions of CE and SE.

Table 1
Accuracy of CE/SE-method

Nr.	L^1-error	EOC	L^2-error	EOC
50	0.002751292	—	0.002384238	—
100	0.000708015	1.96	0.000620088	1.94
200	0.000181108	1.97	0.000163692	1.92
400	0.000046084	1.97	0.000044567	1.88
800	0.000011684	1.98	0.000012461	1.84

method, e.g., point Q in Fig. 1. The set of these points is denoted by Ω. At each grid point, we construct one CE and one associated SE.

The grid points Q, A_1, A_2 A_3 and A_4 are at time level $t = t^n$, where new numerical solutions of flow variables are calculated. Points Q', A'_1, A'_2 A'_3 and A'_4 are the corresponding points at time level $t=t^{n-1/2}$, and points Q'', A''_1, A''_2 A''_3 and A''_4 are at time level $t = t^{n+1/2}$. We will apply the above rule to all mesh points for denoting the time level, i.e., the superscript $'$ for time $t = t^{n-1/2}$, and superscript $''$ for $t = t^{n+1/2}$. Associated with point Q, the SE(Q) is defined as the union of the horizontal plane segment $A_1A_2A_3A_4$, and the two vertical plane segments $B''_1B'_1B'_3B''_3$ and $B''_2B'_2B'_4B''_4$, see Fig. 1(b).

The CE(Q) associated with the point Q is defined as the cylinder $A_1B_1A_2B_2A_3B_3A_4B_4$ $A'_1B'_1A'_2B'_2A'_3B'_3A'_4B'_4$, see Fig. 1(b). The centroid of the top surface of this CE, i.e., the polygon $A_1B_1A_2B_2A_3B_3A_4B_4$, is used as the solution point, which is point Q. All the variables and their spatial derivative are stored at this point Q. The set of solution points is Ω.

The flow variables are assumed smooth inside the SE, and the structure of the flow solution can be discretized by a prescribed function. Following Chang's approach, here also the flow variables are discretized by the first-order Taylor series expansion. That is, for any $(x, y, z) \in$SE(Q), $w_m(x, y, t)$, $f_m(x, y, t)$ and $g_m(x, y, t)$ are approximated by

$$w^*_m(x, y, t) = (w_m)_Q + (w_{mx})_Q(x - x_Q) + (w_{my})_Q(y - y_Q) + (w_{mt})(t - t^n). \tag{3.2}$$

Similarly one can write expressions for $f^*_m(x, y, t)$ and $g^*_m(x, y, t)$. Here x_Q, y_Q, and t^n are the space–time coordinates of Q. Variables w_m, w_{mx}, w_{my} and w_{mt} on the left-hand side of (3.2) are the discretized variables. If all these values are known, the flow solution structure inside the SE is fully specified. However, the above variables are not totally independent. First, by employing Eq. (2.1), we have

$$(w_{mt})_Q = -(f_{mx})_Q - (g_{my})_Q. \tag{3.3}$$

Secondly, by using chain rule, the spatial and temporal derivatives can be calculated by the corresponding Jacobian matrices multiplied by $(w_{mx})_Q$, $(w_{my})_Q$, or $(w_{mt})_Q$. For example,

$$(f_{mx})_Q = (A_{mn})_Q(w_{nx})_Q, \quad (g_{mx})_Q = (B_{mn})_Q(w_{nx})_Q, \tag{3.4}$$

where $m, n = 1, 2, 3, 4, 5$ and $(A_{mn})_Q$ and $(B_{mn})_Q$ are the elements of the Jacobian matrices of f_m and g_m calculated at Q which are given in Appendix A. It is similar for $(f_{my})_Q$, $(g_{my})_Q$, $(f_{mt})_Q$ and $(g_{mt})_Q$. As a result, the only independent discrete variables in each SE are $(w_m)_Q$, $(w_{mx})_Q$, and $(w_{my})_Q$. Once these three variables are calculated, the flow solution structure inside the SE is completely determined.

3.2. The calculation of flow variables w_m

In order to derive the scheme, we replace the continuous space–time flux vector $h_m(x, y, t)$ by a discrete one

$$\mathbf{h}^*_m(x, y, t) = (f^*_m(x, y, t), g^*_m(x, y, t), w^*_m(x, y, t)), \tag{3.5}$$

and the space–time conservation equation (3.1) by its discrete counterpart:

$$\oint_{S(CE(Q))} \mathbf{h}^* \cdot d\mathbf{S} = 0. \tag{3.6}$$

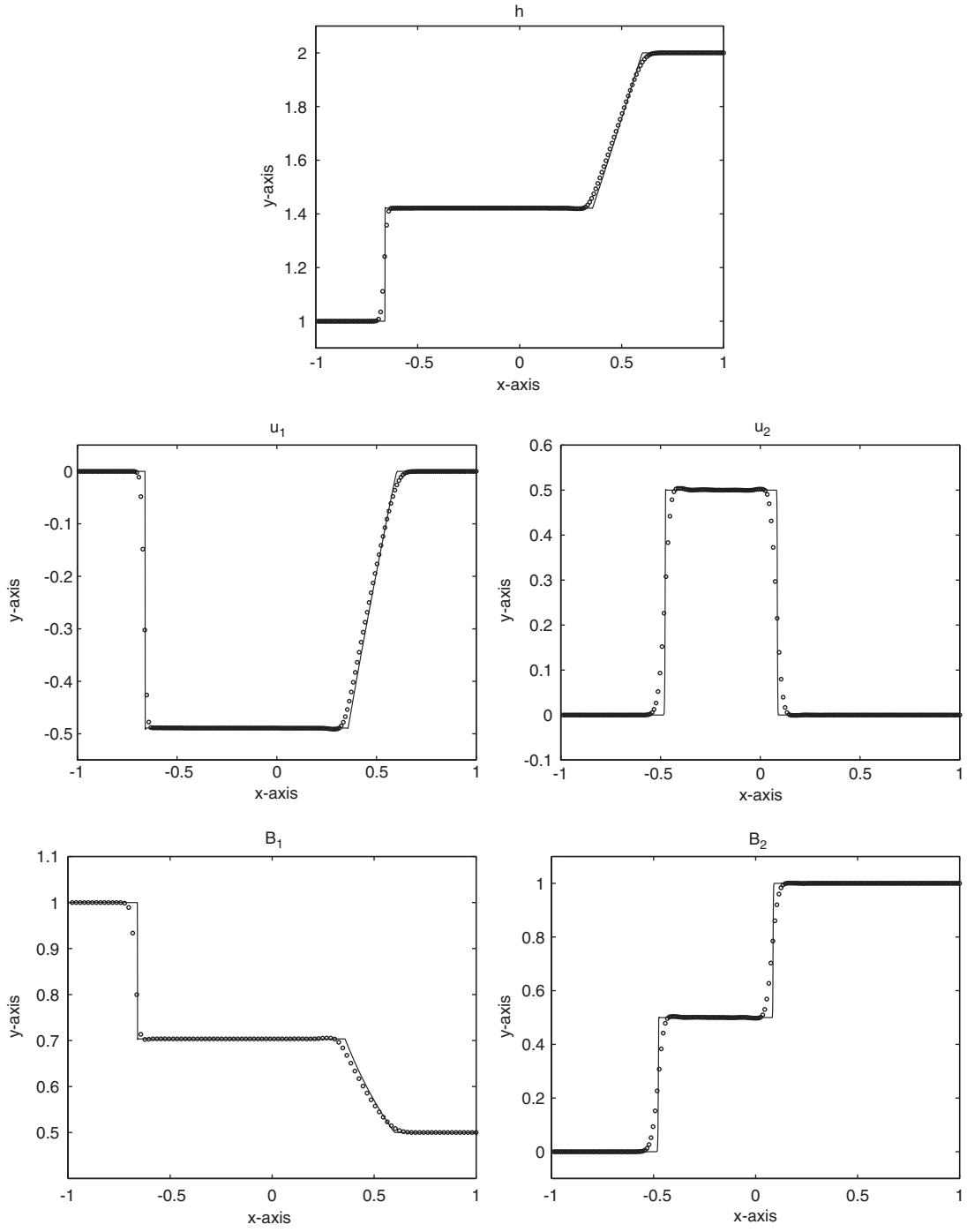

Fig. 2. Results of problem 2 at time $t = 0.4$.

Substituting (3.2)–(3.5) into (3.6), we obtain the algebraic equation,

$$(w_m)_Q^n = \left(\sum_{l=1}^{4} R_m^{(l)} \right) \Big/ S, \tag{3.7}$$

where

$$R_m^{(l)} = S_q^{(l)}[(w_m)_{A_l}^{n-1/2} + (x_q^{(l)} - x_{A_l})(w_{mx})_{A_l}^{n-1/2} + (y_q^{(l)} - y_{A_l})(w_{my})_{A_l}^{n-1/2}]$$
$$- \sum_{k=1}^{2} n_{kx}^{(l)}[(f_m)_{A_l}^{n-1/2} + (x_k^{(l)} - x_{A_l})(f_{mx})_{A_l}^{n-1/2} + (y_k^{(l)} - y_{A_l})(f_{my})_{A_l}^{n-1/2}$$
$$+ \Delta t/4 \cdot (f_{mt})_{A_l}^{n-1/2}] - \sum_{k=1}^{2} n_{ky}^{(l)}[(g_m)_{A_l}^{n-1/2} + (x_k^{(l)} - x_{A_l})(g_{mx})_{A_l}^{n-1/2}$$
$$+ (y_k^{(l)} - y_{A_l})(g_{my})_{A_l}^{n-1/2} + \Delta t/4 \cdot (g_{mt})_{A_l}^{n-1/2}], \tag{3.8}$$

where $l = 1, 2, 3, 4$ indicate the spatial flux contribution from the four neighboring points, and $m = 1, 2, 3, 4, 5$ are indicating the five flow equations. Eq. (3.8) will be used to calculate the numerical solution of w_m at point Q. In the following we illustrate the geometrical treatments in (3.7) and (3.8). Now refer again to Fig. 1

1. The spatial coordinates of the four neighboring solution points, i.e., points A_l, are denoted by (x_{A_l}, y_{A_l}) for $l = 1, 2, 3, 4$.
2. $(x_q^{(l)}, y_q^{(l)})$ for $l = 1, 2, 3, 4$, are the spatial coordinates of the centroids of four quadrilaterals $A_1B_1QB_4$, $A_2B_2QB_1$, $A_3B_3QB_2$, and $A_4B_4QB_3$, respectively.
3. $S_q^{(l)}$ for $l = 1, 2, 3, 4$ are surface areas of the four quadrilaterals defined in 2.
4. $\mathbf{n}_k^{(l)} = (n_{kx}^{(l)}, n_{ky}^{(l)}, 0)$ for $l = 1, 2, 3, 4$ and $k = 1, 2$, represent the eight surface vectors of the following eight lateral planes: $A_1'B_4'A_1B_4$, $A_1'B_1'A_1B_1$, $A_2'B_1'A_2B_1$, $A_2'B_2'A_2B_2$, $A_3'B_2'A_3B_2$, $A_3'B_3'A_3B_3$, $A_4'B_3'A_4B_3$, and $A_4'B_4'A_4B_4$, respectively. Note that the surface vector is defined as the unit outward normal vector (outward from the interior of the CE) multiplied by its area.
5. $(x_k^{(l)}, y_k^{(l)}, t^{n-1/4})$ for $l = 1, 2, 3, 4$ and $k = 1, 2$, are the space–time coordinates of centroids of the eight lateral planes defined in 4.
6. S is the area of the polygon $A_1B_1A_2B_2A_3B_3A_4B_4$, which is also the top surface of the present CE.

We remark that (3.7) and (3.8) represent the space–time flux balance over the CE associated with point Q. The first term at the right-hand side of (3.8) is the space–time flux through the bottom of the CE, contributed by the four neighboring cells at the time level $n - 1/2$. The remainder four terms, at the right-hand side of (3.8), are the space–time fluxes through the eight lateral planes of the present CE, and they are calculated by a inner product vector $\mathbf{n}_k^{(l)} = (n_{kx}^{(l)}, n_{ky}^{(l)}, 0)$. The fluxes, calculated by the right-hand side of (3.8), are balanced by the space–time flux through the top surface (with the area S) of the CE. Since linear distribution of the flow variables is assumed, the flux through the top surface is straightforwardly represented by $(u_m)^n$ at central point Q multiplied by its area S. Because all flow conditions at the $n - 1/2$ time level are known, (3.7) and (3.8) are the explicit method for calculating $(w_m)^n$ at point Q.

3.3. Calculation of derivatives w_{mx} and w_{my} of flow variables

A central difference-type reconstruction approach is employed to calculate $(w_{mx})_Q$ and $(w_{my})_Q$, see [2,5,17]. Using Taylor series we can write

$$(w_m')_{A_l}^n = (w_m)_{A_l}^{n-1/2} + \frac{\Delta t}{2}(w_{mt})_{A_l}^{n-1/2}, \quad l = 1, 2, 3, 4. \tag{3.9}$$

This predicted value is actually a linear expansion in time. By using the values of $(w_m)_{A_1}^n$, $(w_m)_{A_2}^n$ and $(w_m)_Q^n$, we can get the first pair of the spatial derivatives of the flow variables, i.e., $w_{mx}^{(1)}$, $w_{my}^{(1)}$ at point Q:

$$w_{mx}^{(1)} = D_{mx}/D, \quad w_{my}^{(1)} = D_{my}/D, \tag{3.10}$$

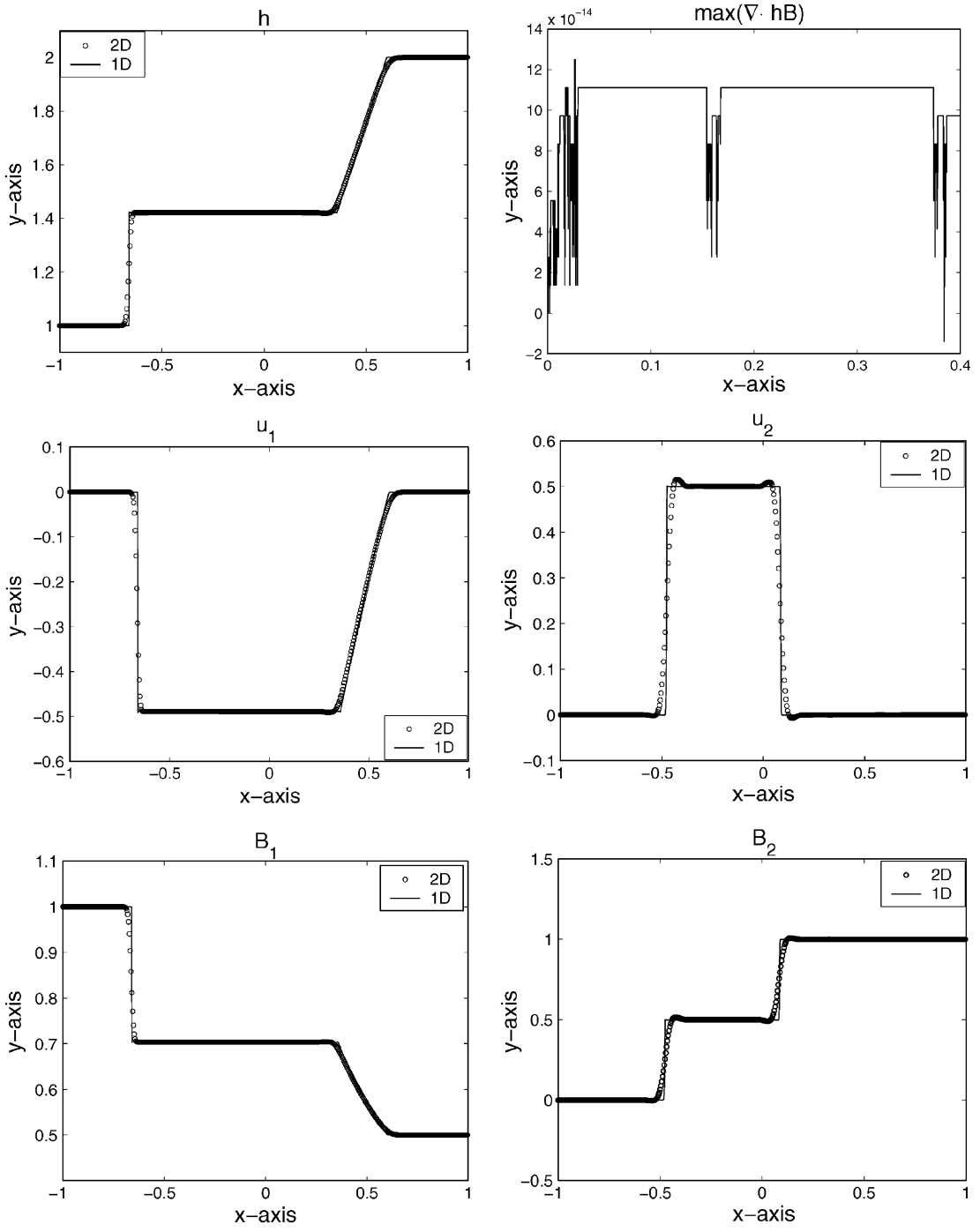

Fig. 3. Results of problem 3 at time $t = 0.4$.

where

$$D = \begin{vmatrix} \Delta x_1 & \Delta y_1 \\ \Delta x_2 & \Delta y_2 \end{vmatrix}, \quad D_{mx} = \begin{vmatrix} \Delta w_m^{(1)} & \Delta y_1 \\ \Delta w_m^{(2)} & \Delta y_2 \end{vmatrix}, \quad D_{my} = \begin{vmatrix} \Delta x_1 & \Delta w_m^{(1)} \\ \Delta x_2 & \Delta w_m^{(2)} \end{vmatrix}, \tag{3.11}$$

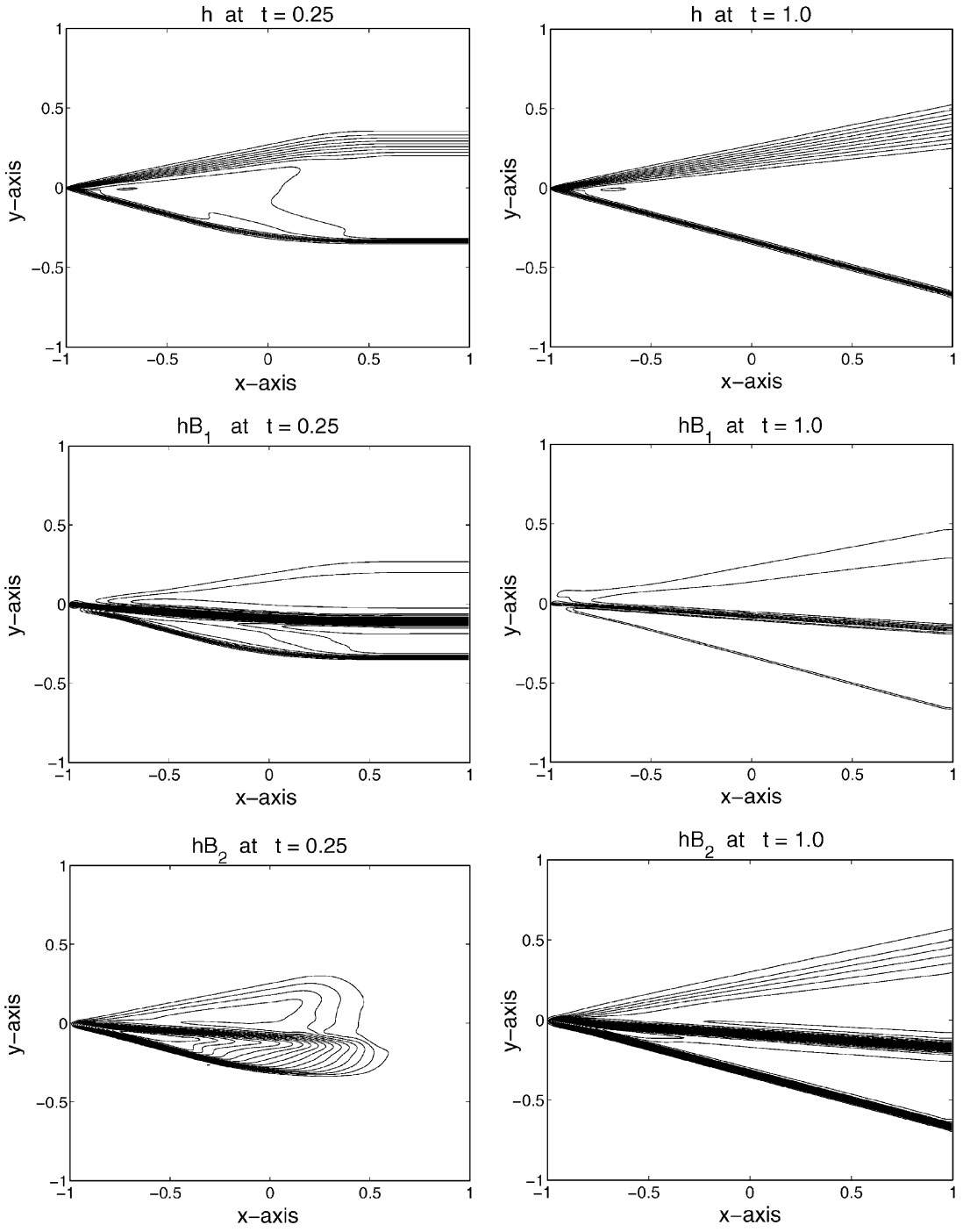

Fig. 4. Results of problem 4.

$$\Delta x_l = (x_{A_l} - x_Q), \quad \Delta y_l = (y_{A_l} - y_Q), \quad \Delta w_m^{(l)} = [(w'_m)^n_{A_l} - (w_m)^n_Q]. \tag{3.12}$$

Similarly, by using solutions at A_2, A_3 and Q, we can get $w_{mx}^{(2)}$, $w_{my}^{(2)}$. By using solutions at A_3, A_4 and Q, we get $w_{mx}^{(3)}$, $w_{my}^{(3)}$. By using solutions at A_4, A_1 and Q, we get $w_{mx}^{(4)}$, $w_{my}^{(4)}$. Finally we calculate w_{mx} and w_{my} at Q by a simple

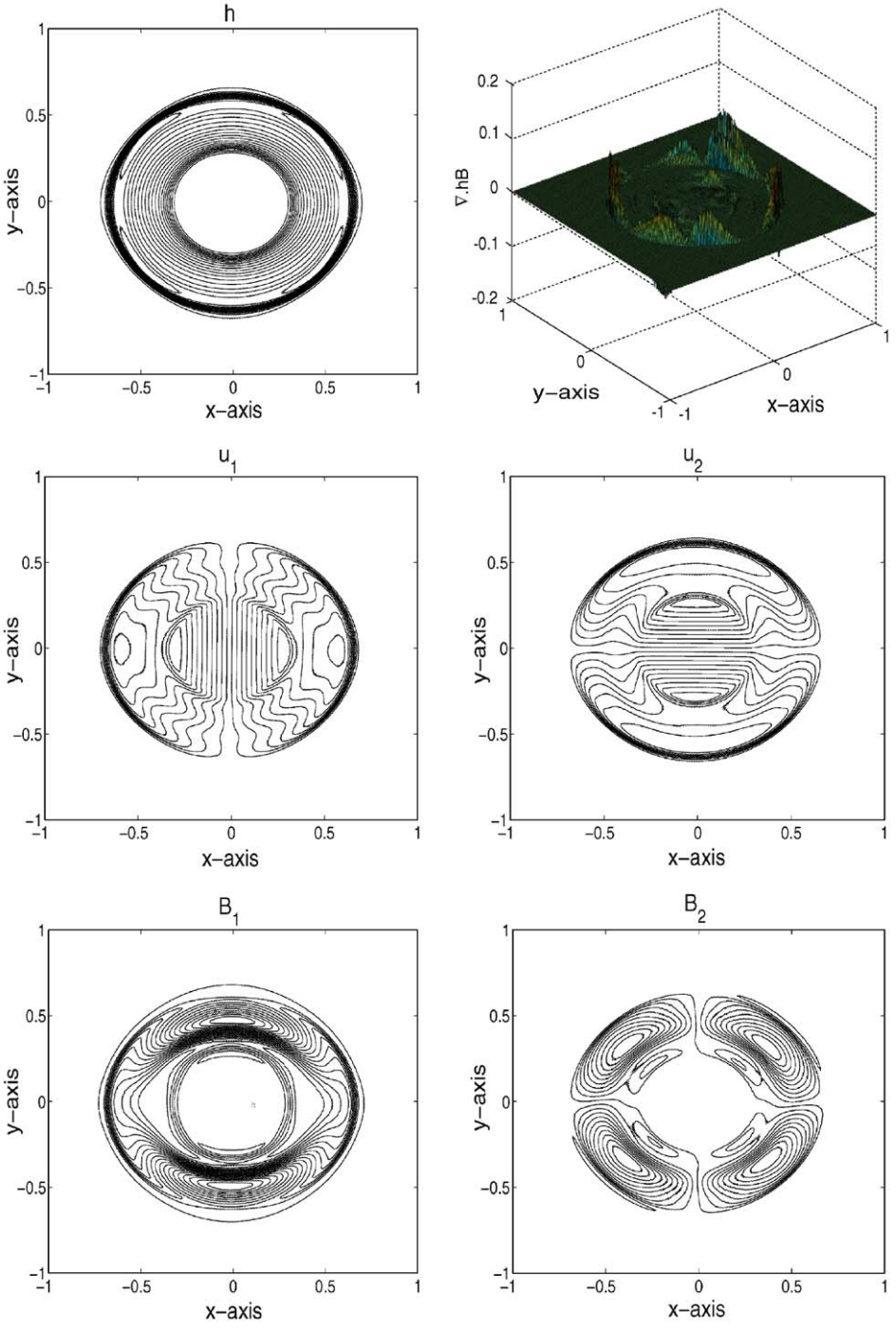

Fig. 5. Two-dimensional rotor-like problem without divergence cleaning on 300 × 300 mesh cells.

average:

$$(w_{mx})_Q^n = \left(\sum_{k=1}^{4} w_{mx}^{(k)}\right) \Big/ 4, \quad (w_{my})_Q^n = \left(\sum_{k=1}^{4} w_{my}^{(k)}\right) \Big/ 4. \tag{3.13}$$

For flows with steep gradients or discontinuities, Eq. (3.13) is modified by re-weighting procedure [2,5,17]:

$$(w_{mx})_Q^n = \begin{cases} 0 \quad \text{if } \theta_{ml} = 0 \quad (l = 1, 2, 3, 4), \\ \sum_{k=1}^{4} [(W_m^{(k)})^\alpha \, w_{mx}^{(k)}] \Big/ \sum_{k=1}^{4} [(W_m^{(k)})^\alpha \text{ otherwise}, \end{cases} \tag{3.14}$$

$$(w_{my})_Q^n = \begin{cases} 0 \quad \text{if } \theta_{ml} = 0 \quad (l = 1, 2, 3, 4) \\ \sum_{k=1}^{4} [(W_m^{(k)})^\alpha \, w_{my}^{(k)}] \Big/ \sum_{k=1}^{4} [(W_m^{(k)})^\alpha \text{ otherwise}, \end{cases} \tag{3.15}$$

where

$$W_m^{(k)} = \prod_{l=1,\ l\neq k}^{4} \theta_{ml}, \quad \theta_{ml} = \sqrt{(w_{mx}^{(l)})^2 + (w_{my}^{(l)})^2}, \tag{3.16}$$

where $l = 1, 2, 3, 4$. In (3.14) α is an adjustable constant, which can be $\alpha = 1$ or 2. However, in all of our numerical test cases we have used $\alpha = 1$. The above modified function is simple and effective to suppress spurious oscillations near shocks. This concludes the formulation of the CE/SE method for SMHD equations at regular rectangular grid. It is to be noted that for the scheme derivation one do not need to take into account any particular hyperbolic system. However, this scheme is not a Jacobian-free and one need to calculate the Jacobian of the fluxes.

It is also important to point out that the scheme used in this article for solving SMHD equations can also be similarly applied to the full ideal MHD equations. Zhang et al. have used CE/SE method in order to solve ideal MHD equations, see [18–20].

4. Numerical case studies

In this section the above prescribed scheme is validated against the typical test cases for SMHD equations available in the current literature. As described in the introduction the one-dimensional version of the present scheme is a special case of the Chang's original scheme [2]. Hence we have not explained the one-dimensional case in this article. However, we present one numerical test case for the one-dimensional SMHD equations as well. In all simulations, unless particularly specified, presented here we use the CFL = 0.5 and the parameter $\alpha = 1.0$.

Problem 1. Experiment order of convergence (EOC).

In order to test the experimental order of convergence of the method we consider a scalar linear hyperbolic equation

$$w_t + w_x = 0 \quad \text{with initial data} \quad w(x, 0) = \sin(\pi x).$$

Here $x \in [0, 2]$, CFL = 0.4 and the final time $t = 2.0$. We use periodic boundary conditions. Table 1 shows the L^1- and L^2-errors between the exact and numerical solutions as well as the experimental order of convergence (EOC).

Problem 2. 1D Riemann problem.

This problem was studied in [9,12,7]. The initial data are

$$x \leqslant 0: \quad h = 1, \quad \mathbf{u} = (0, 0), \quad \mathbf{B} = (1, 0),$$
$$x > 0: \quad h = 2, \quad \mathbf{u} = (0, 0), \quad \mathbf{B} = (0.5, 1),$$

and the gravitational constant $g = 1$. The numerical solution with 100 cells is shown in Fig. 2. The reference solution, solid line, was obtained with the same scheme on 4000 mesh cells. In Fig. 2, the 1-magnetogravity wave appear as a left traveling shock and 4-magnetogravity wave as a right traveling rarefaction. The results obtained have comparable accuracy to that in [12]. Furthermore, our results are completely free of any oscillations near the Alfvén discontinuity. Note that the intrinsic divergence constraint, i.e. $(\nabla \cdot h\mathbf{B}) = 0$, is automatically maintained in the one-dimensional case, see (2.2).

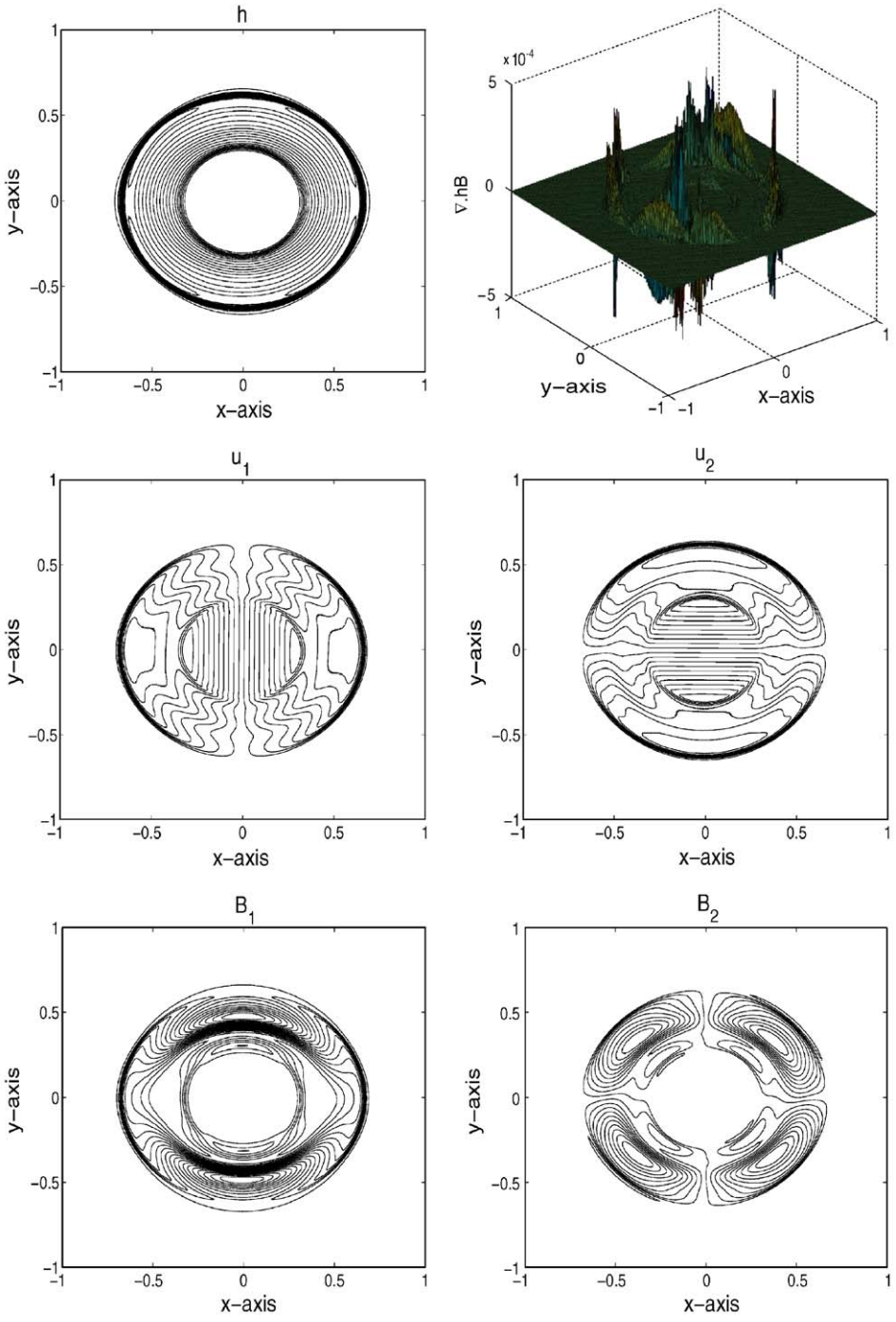

Fig. 6. Two-dimensional rotor-like problem with divergence cleaning on 300 × 300 mesh cells.

Problem 3. Coordinate aligned shock.

This test case is a coordinate aligned shock tube problem as considered above in problem 1. We solve this problem on the domain $(x, y) \in [-1, 1] \times [-1, 1]$ with 200×200 points. The solution of the scheme at $y =$ constant is given

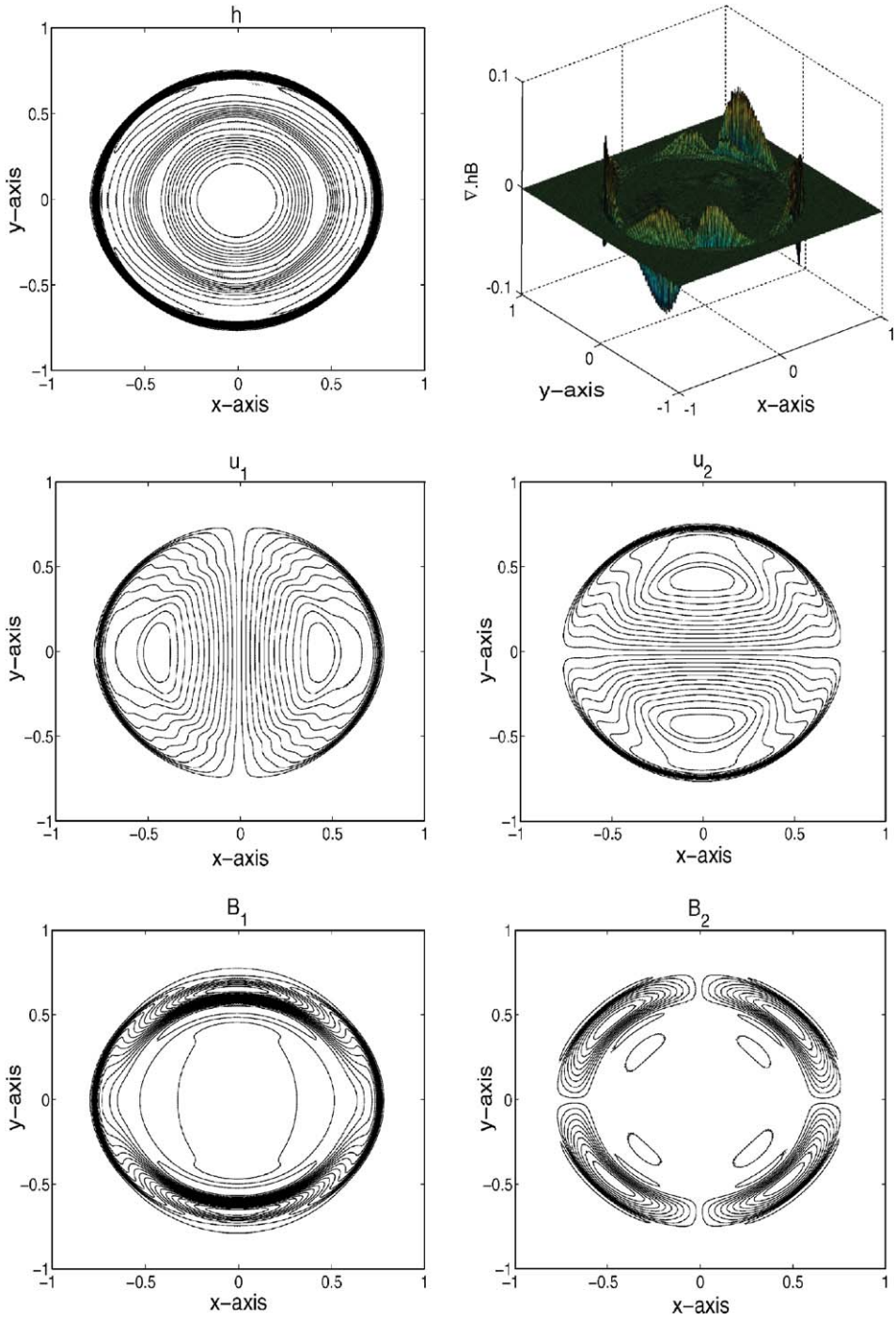

Fig. 7. Results of Problem 6 without divergence cleaning on 300×300 cells at $t = 0.15$.

in Fig. 3 which is also compared with the one-dimensional solution at very fine mesh. As observed in [12], we also see small oscillations in the u_2 profile. In this problem we have not used the divergence cleaning process. Furthermore, our results are completely free of any oscillations near the Alfvén discontinuity which were observed in [9]. The second plot in Fig. 3 shows that the maximum value of the $\nabla \cdot h\mathbf{B}$ is of the order of 10^{-14} throughout the simulation time.

Problem 4. Multidimensional steady-state shock.

This problem was studied in [12,7]. The computational domain is the square box $(x, y) \in [-1, 1] \times [-1, 1]$. The initial data are

$$\mathbf{w}(x, y, 0) = \begin{cases} \mathbf{w}_- & \text{if } y \leqslant 0, \\ \mathbf{w}_+ & \text{if } y > 0, \end{cases} \tag{4.1}$$

where

$$\mathbf{w}_- = \begin{pmatrix} h \\ u_1 \\ u_2 \\ B_1 \\ B_2 \end{pmatrix}_- = \begin{pmatrix} 1 \\ 4.5 \\ 0 \\ 2 \\ 0 \end{pmatrix} \quad \text{and} \quad \mathbf{w}_+ = \begin{pmatrix} h \\ u_1 \\ u_2 \\ B_1 \\ B_2 \end{pmatrix}_+ = \begin{pmatrix} 2 \\ 5.5 \\ 0 \\ 0.5 \\ 0 \end{pmatrix}. \tag{4.2}$$

The boundary conditions on the top, bottom, and right sides are set to outflow, while at the left boundary we impose an inflow boundary condition given by

$$\mathbf{w}(0, y, t) = \begin{cases} \mathbf{w}_- & \text{if } y \leqslant 0, \\ \mathbf{w}_+ & \text{if } y > 0, \end{cases} \tag{4.3}$$

where $\mathbf{w}_-$ and $\mathbf{w}_+$ are again given by (4.2). The computational time is $t = 1$, at which point system has reached its steady state. We take $g = 1$ in this problem.

The results obtained in [12] for this problem work well. Our results are also oscillations free and the method work well like those in [12,7] as given in Fig. 4. We also emphasize that we have again not used any divergence cleaning procedure here. Thus the present scheme is very stable and give comparable accurate results for this particular problem.

Problem 5. Rotor-like problem.

This problem was considered in [9]. This two-dimensional example is similar to the "rotor problem" used in [15] for the MHD equations. The computational domain is $(x, y) \in [-1, 1] \times [-1, 1]$ with extrapolation boundaries. The initial data are

$$\begin{aligned} r \leqslant 0.02: &\quad h = 10, \quad \mathbf{u} = (-y, x), \quad \mathbf{B} = (0.1, 0), \\ r > 0.02: &\quad h = 1, \quad \mathbf{u} = (0, 0), \quad \mathbf{B} = (1, 0), \end{aligned}$$

and the gravitational constant is $g = 1$. Note that $h\mathbf{B}$ is constant in the initial data and thus divergence-free. The results are shown in Figs. 5 and 6 and are comparable to those obtained by using evolution Galerkin schemes [9]. Fig. 5 shows the results from CE/SE method without divergence cleaning procedure, while Fig. 6 shows the results from CE/SE method with divergence cleaning procedure. One can see in Fig. 5 that $\nabla \cdot h\mathbf{B}$ is of the order 10^{-1}, while in Fig. 6 few iterations of projection method have reduced $\nabla \cdot h\mathbf{B}$ to the order 10^{-4}. However, still both results in Figs. 5 and 6 are almost similar. This may be due to the fact that the discrete divergence $\nabla \cdot h\mathbf{B}$ in Fig. 5 is not so large to effect considerably the numerical results. In order to minimize the computational time, we have only iterated the divergence cleaning procedure until $\nabla \cdot h\mathbf{B}$ reduces to the order of 10^{-4}. However, one can reduce this tolerance further at the cost of more computational time. Furthermore, there is no big change in tolerance when one change the number of grid points.

Problem 6. Two separated conducting fluids.

The computational domain is a square region $(x, y) \in [-1, 1] \times [-1, 1]$ with extrapolation boundaries. In the center of the square is a cylindrical region of radius 0.1. The initial data for the fluids in the circular and outside regions are:

$$\begin{aligned} r \leqslant 0.1: &\quad h = 10, \quad \mathbf{u} = (0, 0), \quad \mathbf{B} = (0.1, 0), \\ r > 0.1: &\quad h = 1, \quad \mathbf{u} = (0, 0), \quad \mathbf{B} = (1, 0), \end{aligned}$$

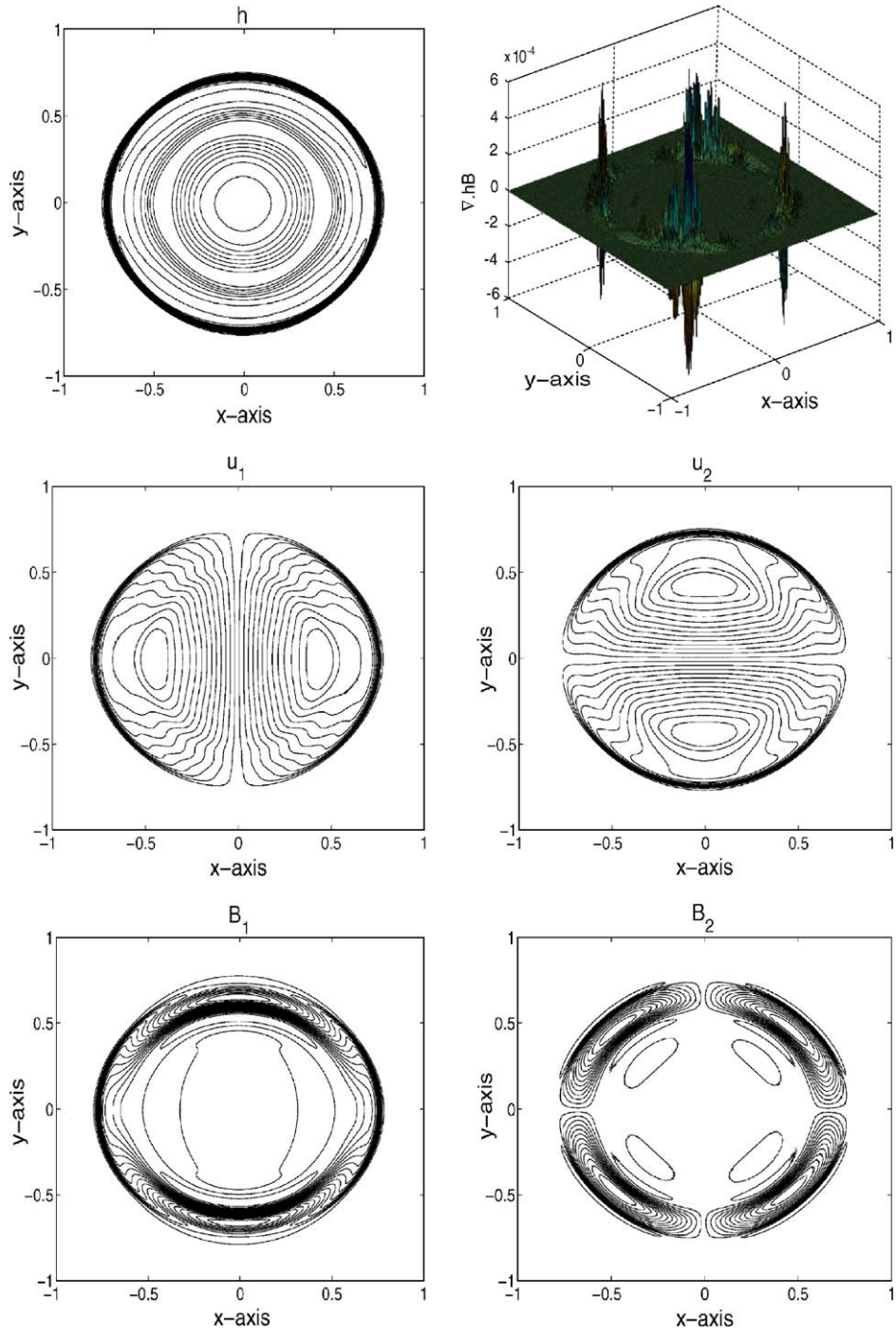

Fig. 8. Results of Problem 6 with divergence cleaning on 300×300 cells at $t = 0.15$.

where the gravitational constant is $g = 1$ and the final time is $t = 0.15$. Suddenly the circular wall making the circular region disappears and the evolution of fluid moment is calculated. Note that $h\mathbf{B}$ is constant in the initial data and thus divergence-free. Here we also present the results without and with divergence cleaning procedure which are given in Figs. 7 and 8, respectively. The behavior of the results is again very similar to those in Problem 5.

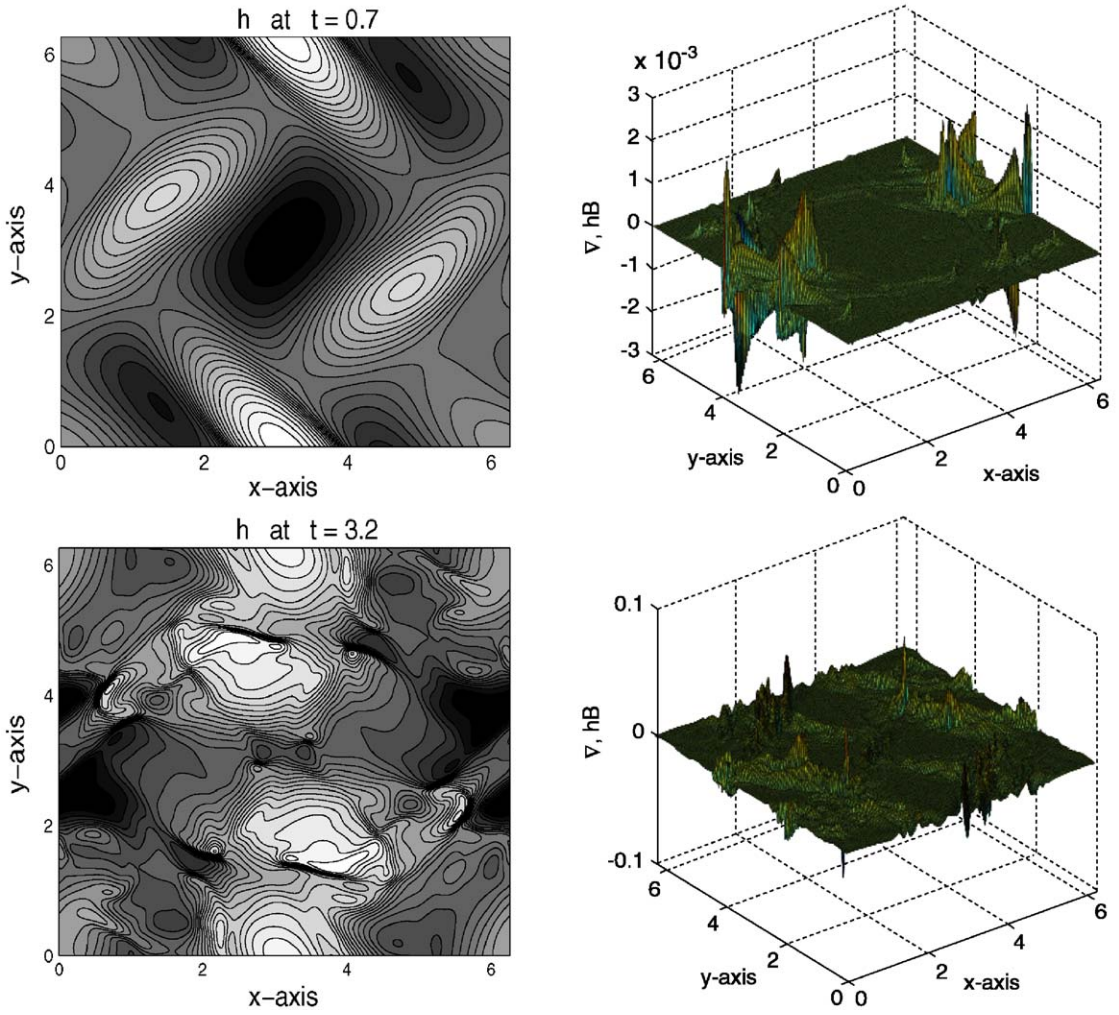

Fig. 9. Results without divergence cleaning at $t = 0.7$ (upper) and $t = 3.2$ (lower).

Problem 7. Orszag–Tang-like turbulance problem.

In this problem, we consider the evolution of a turbulance problem which is analogous to the one studied in [11] for MHD case. It contains many significant features of MHD turbulence which involves the interactions between shock waves which are generated as the vortex system evolves. The computational domain in this case is $(x, y) \in [0, 2\pi] \times [0, 2\pi]$ with periodic boundary conditions on all four sides. The initial data are

$$h(x, y, 0) = \gamma, \quad u_1(x, y, 0) = -\sin\, y, \quad u_2(x, y, 0) = \sin\, x,$$
$$B_1(x, y, 0) = -\sin\, y, \quad B_2(x, y, 0) = -\sin\, 2x.$$

We study this problem by using our scheme with and without imposing the divergence-free procedure. The results with and without divergence cleaning procedure on 300×300 grid points at time $t = 0.7$ and 3.2 are shown in Figs. 9 and 10, respectively. In both cases, the results for the fluid height h are almost the same. One can see in Fig. 9 that $\nabla \cdot h\mathbf{B}$ for the two different final times are of the orders 10^{-3} and 10^{-1}, hence one may conclude that divergence cleaning

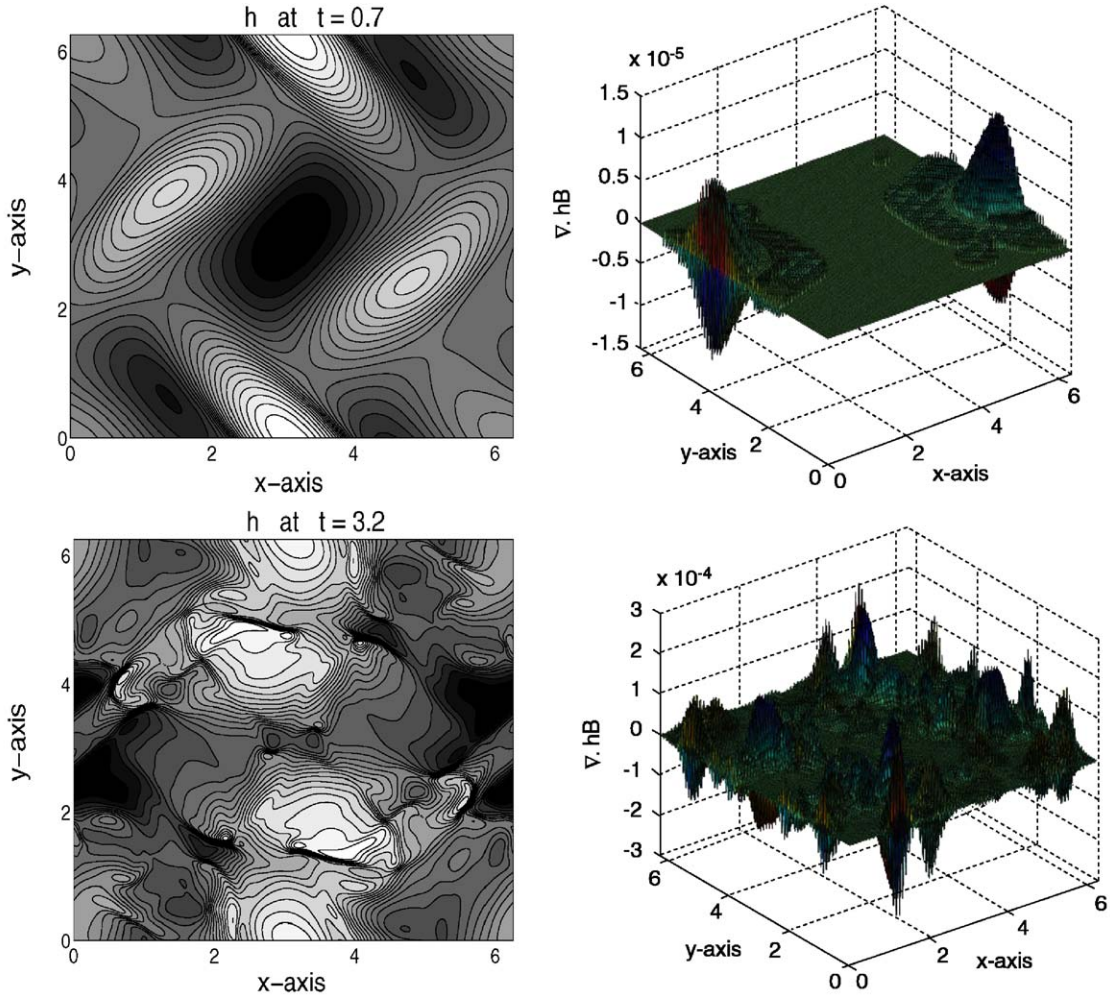

Fig. 10. Results with divergence cleaning at $t = 0.7$ (upper) and $t = 3.2$ (lower).

procedure is not necessary for this problem. With divergence free procedure we have further reduced $\nabla \cdot h\mathbf{B}$ up to the orders 10^{-5} and 10^{-4}, respectively.

5. Conclusions

In this paper we have applied a variant of the CE/SE method, proposed in [17] for the numerical solution of shallow water magnetohydrodynamic (SMHD) equations. The scheme employ only one CE at each grid point in one, two and three space dimensions. From the numerical results, we found that the method perform very well for the present system. Although the discrete divergence of the magnetic field is not satisfied by the scheme, the results obtained with and without divergence cleaning procedure are still very similar. It may be due to the fact that the discrete divergence in all the problems presented in this article are small enough that it does not considerably effect the numerical results. However, there may exist some problems where one must use the divergence cleaning procedure in order to avoid numerical oscillations and negative values of h. Hence it will be better to use divergence cleaning procedure in order to satisfy the divergence constraint up to sufficient accuracy, for example up to the order 10^{-4}. In this article we have used the projection method which worked quite well for the present SMHD system. In summary, the method is suitable for the present model and the results are very encouraging.

Appendix A. The Jacobian matrices in two dimensions

$$A_{mn} = \begin{pmatrix} 0 & 1 & 0 & 0 & 0 \\ -u_1^2 + B_1^2 + gh & 2u_1 & 0 & -2B_1 & 0 \\ -u_1u_2 + B_1B_2 & u_2 & u_1 & -B_2 & -B_1 \\ 0 & 0 & 0 & 0 & 0 \\ -u_1B_2 + u_2B_1 & B_2 & -B_1 & -u_2 & u_1 \end{pmatrix}. \tag{A.1}$$

Similarly

$$B_{mn} = \begin{pmatrix} 0 & 0 & 1 & 0 & 0 \\ -u_1u_2 + B_1B_2 & u_2 & u_1 & -B_2 & -B_1 \\ -u_2^2 + B_2^2 + gh & 0 & 2u_2 & 0 & -2B_1 \\ -u_2B_1 + u_1B_2 & -B_2 & B_1 & u_2 & -u_1 \\ 0 & 0 & 0 & 0 & 0 \end{pmatrix}. \tag{A.2}$$

References

[1] J.U. Brackbill, D.C. Baranes, The effect of nonzero $\nabla \cdot \mathbf{B}$ on the numerical solution of the magnetohydrodynamic equations, J. Comput. Phys. 35 (1980) 426–430.

[2] S.C. Chang, The method of space time conservation element and solution element—a new approach for solving the Navier Stokes and Euler equations, J. Comput. Phys. 119 (1995) 234–295.

[3] S.C. Chang, Courant number insensitive CE/SE schemes, AIAA Paper 2002–3890 (2002).

[4] S.C. Chang, X.Y. Wang, Multi-dimensional courant number insensitive CE/SE Euler solvers for applications involving highly nonuniform meshes, AIAA Paper 2003–5285 (2003).

[5] S.C. Chang, X.Y. Wang, C.Y. Chow, New developments in the method of space–time conservation element and solution element—applications to two-dimensional time-marching problems, NASA TM 106758, December 1994.

[6] S.C. Chang, X.Y. Wang, C.Y. Chow, The space–time conservation element and solution element method: a new high resolution and genuinely multidimensional paradigm for solving conservation laws, J. Comput. Phys. 156 (1999) 89.

[7] H. De Sterck, Hyperbolic theory of the shallow water magnetohydrodynamics, Phys. Plasmas 8 (2001) 3293–3304.

[8] P.A. Gilman, Magnetohydrodynamic shallow water equations for the solar tachocline, Astrophys. J. Lett. 544 (2000) 79–82.

[9] T. Kröger, M. Lukáčová-Medvidová, An evolution Galerkin scheme for the shallow water magnetohydrodynamic (SMHD) equations in two space dimensions, J. Comput. Phys. 206 (2005) 122–149.

[10] M. Lukáčová-Medvid'ová, M. Saibertova, Genuinely multidimensional evolution Galerkin scheme for the shallow water equations, in: F. Brezzi et al. (Eds.), Numerical Mathematics and Advanced Applications, World Scientific Publishing Company, Singapore, 2002, pp. 105–114.

[11] S.A. Orszag, C.M. Tang, Small-scale structure of two-dimensional magnetohydrodynamic turbulence, Fluid Mech. J. 90 (1979) 129.

[12] J.A. Rossmanith, A wave propagation method with constrained transport for ideal and shallow water magnetohydrodynamics, Ph.D. Thesis, University of Washington, Seattle, Washington, 2002.

[13] E.A. Spiegel, J.-P. Zahn, The solar tachocline, Astron. Astrophys. 265 (1992) 106–114.

[14] E.F. Toro, Shock-capturing Methods for Free Surface Shallow Fluids, vol.2, Wiley, New York, 1962.

[15] G. Tóth, The $\nabla \cdot \mathbf{B} = 0$ constraint in shock-capturing magnetohydrodynamics codes, J. Comput. Phys. 161 (2000) 605–652.

[16] X.Y. Wang, C.Y. Chow, S.C. Chang, Application of the space–time conservation element and solution element method to two-dimensional advection–diffusion problems, NASA TM 106946, June 1995.

[17] Z.-C. Zhang, S.T. Yu, S.C. Chang, A space–time conservation element and solution element method for solving the two-dimensional unsteady Euler equations using quadrilateral and hexahedral meshes, J. Comput. Phys. 175 (2002) 168–199.

[18] Z.-C. Zhang, S.T. Yu, S.C. Lin, S.C. Chang, I. Blankson, Solving the MHD equations by the CE/SE method with and without a projection method for Div B = 0, AIAA J. 42(12) (2004) 311–326, 2605–2608.

[19] Z.-C. Zhang, S.T. Yu, S.C. Lin, Solving the MHD equations by the CE/SE method with and without a projection method for Div B = 0, Trans. Aeronautical Astronautical Soc. Republic China 36 (2004) 311–326.

[20] Z.-C. Zhang, S.T. Yu, S.C. Lin, S.C. Chang, I. Blankson, Application of the space–time conservation element and solution element method to the ideal magnetohydrodynamics equations, AIAA Paper 2002–3888, 2004.